A One-Equation Turbulence Model for Aerodynamic Flows

Article · January 1992

DOI: 10.2514/6.1992-439

2 authors:

Philippe Spalart
The Boeing Company
251 PUBLICATIONS **36,080** CITATIONS
SEE PROFILE

Steven Allmaras
Massachusetts Institute of Technology
68 PUBLICATIONS **12,873** CITATIONS
SEE PROFILE

La Recherche Aérospatiale, 1994, n° **1**, 5-21

A one-equation turbulence model for aerodynamic flows (*)

P. R. Spalart [1] and S. R. Allmaras [1]

(*) *Originally presented at the AIAA 30th Aerospace Sciences Meeting and Exhibit, 6-9 January, 1992, Reno, NV, USA.*
[1] *Boeing Commercial Airplane Group. P.O. Box 3707, MS 7H-96. Seattle, WA 98124-2207, USA.*

Manuscript received March 27, 1992; accepted May 3, 1993.

Spalart P. R., Allmaras S. R., *La Recherche Aérospatiale*, 1994, n° **1**, 5-21

Résumé

Modélisation d'écoulements aérodynamiques turbulents par une équation unique. Une équation de transport de la viscosité turbulente est assemblée de manière empirique, à l'aide d'arguments d'analyse dimensionnelle, d'invariance galiléenne et de dépendance sélective par rapport à la viscosité moléculaire. Le modèle ressemble à ceux de Nee et Kovasznav, de Secundov *et al.* et de Baldwin et Barth. L'équation comporte un terme non visqueux de destruction qui est fonction de la distance à la paroi. Contrairement aux modèles algébriques et aux premiers modèles à une équation, celui-ci est ponctuel. En effet, la solution de l'équation en un point ne dépend pas de celles en d'autres points. Ce modèle convient donc à toute structure de maillage. En outre, il est numériquement souple en ce qui concerne la résolution et la raideur au voisinage de la paroi. Les conditions limites à la paroi et dans l'écoulement libre sont triviales. Le modèle donne une transition laminaire-turbulente relativement lisse aux points définis par l'utilisateur. Un simple « indice de turbulence » est donné pour déterminer les régions de la couche limite où le modèle est actif. Il est étalonné sur des zones de mélange, des sillages et des couches limites de plaque mince. La prévision des couches limites dans les gradients de pression est en assez bon accord avec les résultats expérimentaux. Des solutions des équations Navier-Stokes stationnaires bidimensionnelles sont présentées, avec un décollement provoqué par un choc, et avec un bord de fuite émoussé. Ce modèle situe les chocs légèrement en amont par rapport au modèle de Johnson et King. Il fonctionne bien dans le sillage proche et donne des résultats prometteurs pour des écoulements plus complexes. Des résultats allant de moyens à bons ont déjà été obtenus par 8 équipes différentes, y compris dans le cas de profils hypersustentateurs et de voilures transsoniques.

Mots-clés : *(lexique CEDOCAR)* : Turbulence – Viscosité – Modèle mathématique – Équation transport – Mélange turbulent – Sillage turbulent – Couche limite.

Abstract

A transport equation for the turbulent viscosity is assembled, using empiricism and arguments of dimensional analysis, Galilean invariance, and selective dependence on the molecular viscosity. It has similarities with the models of Nee and Kovasznay, Secundov *et al.*, and Baldwin and Barth. The equation includes a non-viscous destruction term that depends on the distance to the wall. Unlike algebraic and early one-equation models the new model is local, in the sense that the equation at one point does not depend on the solution at other points. It is therefore compatible with grids of any structure. It is numerically forgiving, in terms of near-wall resolution and stiffness. The wall and freestream boundary conditions are trivial. The model yields relatively smooth laminar-turbulent transition, at points specified by the user. A simple "turbulence index" is provided to determine the regions of a boundary layer in which the model is active. The model is calibrated on 2-D mixing layers, wakes, and flat-plate boundary layers. It yields satisfactory predictions of boundary layers in pressure gradients. Two-dimensional steady-state Navier-Stokes solutions are presented, including shock-induced separation and a blunt trailing edge. The model locates shocks slightly farther forward than the Johnson-King model. It performs well in the near wake and appears to be a good candidate for more complex flows. It has now been implemented by eight separate groups; the results range from fair to good, including cases of high-lift airfoils and transonic wings.

Keywords: *(NASA thesaurus)*: Turbulence-viscosity – Mathematical models – Transport equation – Turbulent mixing – Turbulent wakes – Boundary layers.

LIST OF SYMBOLS

c_{b1}, etc.	empirical constants in the turbulence model
c	chord of an airfoil
$C_f \equiv 2\,(u_\tau/U)^2$	skin-friction coefficient
C_p	pressure coefficient
C_l	lift coefficient
d	distance to the wall
f_{v2}, etc.	empirical functions in the turbulence model
g, r, $\tilde{S}$	intermediate variables
$H \equiv \delta^*/\theta$	shape factor
k	turbulent kinetic energy
l	mixing length
M	freestream Mach number
Re	chord Reynolds number
$\mathrm{R}_\theta \equiv \theta\, U_{\mathrm{edge}}/\nu$	momentum-thickness Reynolds number
$S_{ij} \equiv (\partial U_i/\partial x_j + \partial U_j/\partial x_i)/2$	strain-rate tensor
S	measure of the deformation tensor
t	time
$u_\tau \equiv \sqrt{\nu\, \partial U/\partial y\,(y=0)}$	friction velocity
u_i	fluctuating velocity components
U	mean velocity in x direction
U_i	mean velocity components
U_{edge}	edge velocity of boundary layer
U_∞	freestream velocity for airfoil
x	streamwise coordinate
x_i	Cartesian coordinates
y	distance to the wall
$y^+ \equiv y u_\tau/\nu$	wall variable
α	direction of the deformation tensor
δ	thickness of the shear layer
δ^*	displacement thickness
ϵ	turbulent dissipation rate
κ	Kármán constant, taken as 0.41
ν	kinematic molecular viscosity
ν_t	kinematic turbulent, or eddy, viscosity
$\tilde{\nu}$	working variable of the turbulence model
$\omega \equiv \sqrt{\Omega_{ij}\,\Omega_{ij}}$	vorticity
$\Omega_{ij} \equiv \partial U_i/\partial x_j - \partial U_j/\partial x_i$	rotation tensor
σ	turbulent Prandtl number
θ	momentum thickness
τ	shear stress
$\chi \equiv \tilde{\nu}/\nu$	intermediate variable

I – MOTIVATION AND RELATED WORK

The aerodynamics community is ready to invest in a new generation of turbulence models, more onerous than the algebraic models but with a wider envelope in terms of flow and grid complexity. The Baldwin-Lomax model [1] made Navier-Stokes calculations possible in situations that are awkward for the Michel and Cebeci-Smith models [2, 3], because the thicknesses of the boundary layer are not well defined. The Johnson-King model [4] has by-and-large fulfilled the demand for more accurate prediction of shock/boundary-layer interactions, compared with the purely algebraic models. However these models, even when used in Navier-Stokes codes, are boundary-layer models in spirit. Physically, they treat the whole boundary layer as a single, tightly-coupled module, which becomes incorrect when detached and multiple shear layers are present. They rely on surveying the velocity or vorticity profile on a smooth grid line, roughly orthogonal to the surface, thus being "non-local". This becomes expensive and awkward when an unstructured grid is used [5]. Even when the only complication is that two solid bodies are present, implementing an algebraic model requires decisions that border on artificial intelligence and cannot be fully automated. In addition, multi-block and unstructured-grid methods are becoming more common. Finally, we do not know of an algebraic model that ensures continuity of the eddy viscosity between the airfoil block and the wake block, in a C-grid setting, while offering a plausible formula in the wake. This is disturbing, and it can cause stability problems [6]. Some methods incorporate a blending of the two formulas, this mimicking a transport equation. However, it is done along grid lines, which are arbitrary.

Transport-equation models such as k-ϵ and higher models are usually "local", although some have non-local near-wall terms, and have been available for years. However, they are far from having shown a decisive advantage for the prediction of shock/boundary-layer interactions or separation from smooth surfaces [7]. They are also much more difficult

to use. This is not so much because of the extra storage, but because they require finer grids near a wall, involve strong source terms that often degrade the convergence, and demand non-trivial upstream and freestream conditions for the turbulence variables. The near-wall problems often lead to the use of wall functions, which are unwieldy and lose any justification in the situation that matters most, namely, separation.

The recent Baldwin-Barth model [8, 9] is an attractive intermediate. It has only one equation and is local, except for the y^+ dependence which they plan to dispose of in the long term (B. Baldwin, personal communication). It is derived from the k-ϵ model, through some further assumptions. Near the wall it does not require finer resolution than the velocity field itself. Depending on the version, it predicts adverse-pressure-gradient cases and shock interactions better than Baldwin-Lomax, but not consistently as well as Johnson-King, as shown by Menter [10]. Its accuracy will improve in time, and it is much more practical than two-equation models.

The present project was prompted by Baldwin and Barth's work, and by the belief that generating a one-equation model as a simplified version of the k-ϵ model is not optimal. A one-equation model is simple enough that it can be generated "from scratch", which may lead to better performance and certainly gives fuller control over its mechanics. A case in point is the Baldwin-Barth diffusion term, which is constrained by the k-ϵ ancestry and the further assumptions made. We also allow a "semi-local" near-wall term, as described below. Our calibration strategy is different. We expect time to tell that the new model has the same properties as that of Baldwin-Barth in terms of compatibility with unstructured grids and benign near-wall behavior, and is more accurate, especially away from the wall, as well as slightly more robust. For instance, it accepts zero values in the freestream. The improved performance may be traced to a larger number of adjustable constants, but these are all firmly calibrated.

The roster of one-equation models also includes those of Bradshaw, Ferriss and Atwell [11], Nee and Kovasznay [12], Secundov and his co-workers [13], Mitcheltree, Salas and Hassan [14], and Johnston [15]. Except for Secundov's and Baldwin and Barth's, these models are not local, as they use length scales related to the boundary-layer thickness. This contributes to the common claim that one-equation models are not "complete". The Secundov model was entered in the Collaborative Testing of Turbulence Models (CTTM, [16]) and Prof. Bradshaw was kind enough to provide the one-page description that was submitted. Dr. Secundov provided additional details in personal communications as well as a list of publications ranging from 1971 to 1986, all of them in Russian. This model is presented as an evolution of the Nee-Kovasznay model, but is local and rich in near-wall and compressibility corrections. Some versions also have a term designed to fit the round jet, for instance, reflecting both the creativity of that group and their ambition to create a "universal" model. We have a more limited range of flows in mind, as reflected in our title. Note that we have "reinvented" their near-wall destruction term. It is expected for simple empirical models, developed under roughly the same constraints (invariance, etc.), to exhibit strong similarities. However, the leeway is large enough to produce models with widely different performance.

II – PRESENTATION AND CALIBRATION OF THE MODEL

II.1 – Overview

The model has four nested versions from the simplest, applicable only to free shear flows, to the most complete, applicable to viscous flows past solid bodies and with laminar regions. As each additional physical effect is considered, new terms or factors are introduced and calibrated. They are identified by a common letter subscript in the constants and functions involved. The new terms are passive in all the lower versions of the model, so that the calibration proceeds in order. This presentation may seem heavy, but should instructive as it allows the readers to critique the theory or the calibration shell by shell and to test the relevant version in the situation of their choice. It should also help preserve some clarity in later alterations of the model. The Appendix gives the equations for the complete model.

II.2 – Free shear flows

The central quantity is the eddy viscosity ν_t; the Reynolds stresses are given by the constitutive relation $-\overline{u_i\, u_j} = 2\nu_t S_{ij}$. There is no exact transport equation for ν_t which we could approximate term by term. The option of generating a "general" transport equation and calibrating it with a sufficient number of cases is also out of the question, because there is no limit to the nonlinearities and cross-terms between the various influences the turbulence is submitted to. Therefore, we take an empirical approach.

We construct the model by gathering quantities, derived from the mean flow field and from ν_t, which have Galilean invariance. For example, the mean velocity U is not receivable, except of course in the convection term. We then invoke common notions of turbulence – for instance, related to its diffusion – to assemble dimensionally correct terms that together constitute a plausible transport equation for ν_t. In this subsection we consider free shear flows at high Reynolds numbers, and accordingly the molecular viscosity is not allowed in the equation. The left-hand side of the equation is the Lagrangian or material derivative of ν_t : $D\nu_t/Dt \equiv \partial\nu_t/\partial t + U_i\, \partial\nu_t/\partial x_i$.

On the right-hand side we provide a production term and diffusion terms.

For the production term, the deformation tensor $\partial U_i/\partial x_j$ presents itself. Since ν_t is a scalar we seek a scalar measure, denoted by S, of that tensor. $S\nu_t$ then has the desired dimension. We have used the vorticity $|\omega|$ for S. Other plausible combinations would be the strain rate $\sqrt{2\,S_{ij}\,S_{ij}}$ or the norm of the whole tensor $\sqrt{U_{i,j}\,U_{i,j}}$. We normalize any candidate so that it reduces to $|U_y|$ in a simple shear flow. The argument in favor of $|\omega|$ is that, in the flows of interest to us, turbulence is found only where vorticity is present, with both emanating from the solid boundaries. There are regions of vorticity without turbulence behind shocks, but that vorticity is normally too weak to produce much eddy viscosity.

The production term, and in fact the restriction of the model to homogeneous turbulence, is

$$\frac{D\nu_t}{Dt} = c_{b1}\,S\,\nu_t. \qquad (1)$$

The subscript b stands for "basic". The response of the model in homogeneous turbulence is dull, but not grossly inaccurate. The eddy viscosity is stationary in isotropic turbulence (*i.e.*, $D\nu_t/Dt = 0$, because $S=0$). Experiments show that in such a flow the energy k is approximately proportional to $t^{-6/5}$ [17]. Then the simplest combination that has the same dimensions as ν_t, namely k^2/ϵ, slowly decays like $t^{-1/5}$. In anisotropic flows ν_t can only increase under the effect of production, in a manner that depends on the choice of S. That choice may be re-examined later, but if we consider a shear flow with $S \equiv |U_y|$ we observe that ν_t grows exponentially like $\exp(c_{b1}\,S\,t)$. This is the classical behavior for shear flow in the limit of large time, with a growth rate in the 0.10 to 0.16 range according to experiments and direct numerical simulations. Our calibration on inhomogeneous flows yields values of c_{b1} between 0.13 and 0.14. Thus, we do not emphasize homogeneous turbulence, but we are not in strong conflict with it. The Baldwin-Barth and Secundov models have rather large production constants, at least 0.20. Note that we have not found any plausible and invariant quantity that could constitute a destruction term away from walls. We return to this issue later.

The search for diffusion terms naturally focuses on spatial derivatives of ν_t. Classical diffusion operators are of the type $\nabla.([\nu_t/\sigma]\nabla\nu_t)$. They conserve the integral of ν_t, save for boundary contributions. However, there is no reason why the integral of ν_t should be conserved. Manipulations of two-equation models often bring out diffusion terms that are not conservative, for instance cross terms between ∇k and $\nabla\epsilon$. By analogy and to acquire a degree of freedom, we allow a non-conservative diffusion term, involving first derivatives of ν_t. We arrive at the following "basic" model:

$$\frac{D\nu_t}{Dt} = c_{b1}\,S\,\nu_t + \frac{1}{\sigma}\,[\nabla.(\nu_t\,\nabla\nu_t) + c_{b2}\,(\nabla\nu_t)^2]. \qquad (2)$$

We break our convention for σ, which belongs to the c_b series, because of the traditional notation of Prandtl numbers.

The diffusion term of (2) conserves the integral of the quantity $\nu_t^{1+c_{b2}}$. Recall the lack of a destruction term. This lack was responsible for a mild inconsistency in isotropic turbulence (the $t^{-1/5}$ decay). It could also invalidate the model in the class of shear flows in which ν_t decreases (negative $D\nu_t/Dt$) such as an axisymmetric wake. However, the diffusion term can easily bring down the centerline value of ν_t, and the true constraint is that under (2) the integral of $\nu_t^{1+c_{b2}}$ cannot decrease. With the classical exponents of the self-similar turbulent axisymmetric wake (length scale $\propto t^{1/3}$, velocity $\propto t^{-2/3}$), we find that the integral increases provided that $c_{b2} \leq 1$.

A more important constraint is obtained from the behavior of a turbulent front. The diffusion term admits the following (weak) one-dimensional solution:

$$\nu_t\,(x,\,t) = \max\left(0,\,A\left[x + \frac{A\,(1+c_{b2})}{\sigma}\,t\right]\right). \qquad (3)$$

for any constant A. This is a linear ramp propagating at the velocity $-A\,(1+c_{b2})/\sigma$. If $c_{b2} > -1$ it propagates into the non-turbulent region, which is physically correct. The equivalent of c_{b2} is 0 in the Secundov model (*i.e.*, the diffusion term is conservative). It equaled –2 in the original Baldwin-Barth model [8] (*i.e.*, the diffusion term conserves $1/\nu_t$) and is somewhat below –1 in the published version [9], so that under the diffusion term alone the turbulent front recedes. We believe this effect is to blame for the sensitivity of that model to the freestream value of ν_t (or $\tilde{R}_T$). Note that Baldwin and Barth are constrained in their choice of the c_{b2} equivalent by the connection with the k-ϵ model, in the original version, and by their calibration in the log layer, in both versions. We avoid this conflict thanks to a near-wall term as explained below. The solution in (3) is of great interest in practice, as it indeed gives the structure of the solution at the edge of a turbulent region, where the diffusion term dominates (*see Figs. 2, 4, and 6, below*).

The fact that the dependent variable ν_t is its own diffusion coefficient is responsible for the existence of weak solutions such as (3), and raises the possibility of non-unique solutions whenever ν_t takes zero values. Indeed if the initial condition is $|x|$, we have a singular solution in which ν_t behaves like $|x|^{1/(2+c_{b2})}$ near $x=0$, and a smooth solution with $\nu_t > 0$ at $x=0$. The difference is confined to a boundary layer near $x=0$. In a numerical setting with straightforward second-order centered differencing and a point at $x=0$, the weak solution is obtained if the diffusion term is written $\nu_t\,\nabla^2\nu_t + (1+c_{b2})\,(\nabla\nu_t)^2$, but the smooth solution is obtained if it is written as in (2). Other forms that give the smooth solution are $\nabla^2\,(\nu_t^2/2) + c_{b2}(\nabla\nu_t)^2$ and

$(1+c_{b2})\nabla(\nu_t\nabla\nu_t)-c_{b2}\nu_t\nabla^2\nu_t$. The later addition of a term proportional to the molecular viscosity (§ II,4) formally resolves this non-uniqueness and leads to the smooth solution with $\nu_t > 0$. However, particularly at high grid Reynolds numbers, it is desirable to use a favorable form of the diffusion term.

Outside but close to a turbulent shear layer the Reynolds stresses, particularly the diagonal components, do not exactly vanish. However, they are induced by pressure fluctuations and bear little relationship to the local strain tensor. For that reason, it is as well to have the eddy viscosity be zero outside the turbulent region, and this is the value we recommend in the freestream. In addition, the model is essentially insensitive to non-zero values (which may help some numerical solvers), provided that they are much smaller than the values in the turbulent region. This is due to the dominance of the turbulent region ($\nu_t > 0$) over the non-turbulent one, as illustrated by the ramp solution (3). This feature adds to the "black box" character of the new model and represents a substantial advantage over the Baldwin-Barth model and many two-equation models, some of which are highly sensitive to freestream values – notably that of the time scale.

We now discuss the amplification of the eddy viscosity by the production term, which is the only one preserved by the linearization of (2) for small ν_t. Consider the steady flow at a velocity U_∞ past a body of size L, with thin shear layers of thickness δ. Outside the shear layers the deformation tensor is of order U_∞/L, and particles are subjected to it for a time on the order of L/U_∞ (with the exception of the streamline leading to a stagnation point). Thus, irrespective of the exact definition of S, the logarithm of the amplification ratio will be on the order of c_{b1}, and small values will remain small. In contrast in the thin shear layers near the body the logarithm of the amplification ratio under the effect of the production term alone would be on the order of $c_{b1}L/\delta$, and therefore large in the usual situation since $L \gg \delta$. Thus small values of ν_t, whether inherited from the freestream, or resulting from numerical errors, or introduced intentionally at the "trip" as described later, will cause transition in the thin shear layers only. By transition we mean growth to such levels that the diffusion terms, which are nonlinear, become active (the destruction term introduced later is also nonlinear). The sequence of exponential growth, followed by saturation at levels on the order of $U_\infty\,\delta$, is consistently observed.

We now calibrate the free-shear-flow version of the model by requiring correct levels of shear stress in two-dimensional mixing layers and wakes. Fair values for the peak shear stress are 0.01 $(\Delta U)^2$ in the mixing layer and 0.06 $(\Delta U)^2$ in the wake, where ΔU is the peak velocity difference [17]. This gives two constraints for three free constants c_{b1}, σ, and c_{b2}, and leaves a one-dimensional family of "solutions"

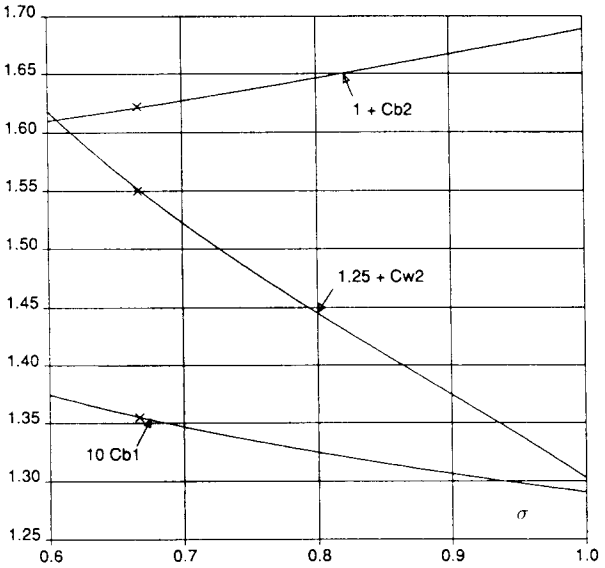

Fig. 1. – Calibrated model constants. — locus of solutions; × point selected for the calculations.

which is shown in *figure 1* parameterized by the Prandtl number, the easiest quantity to interpret. The range of values we consider plausible is $\sigma \in [0.6, 1]$. The corresponding values of c_{b2} are between 0.6 and 0.7 and, fortunately, satisfy our "guidelines" (*i.e.*, $-1 < c_{b2} \leq 1$) with a margin. The constant c_{w2} is introduced in § II,3.

Time-developing mixing-layer and wake solutions were obtained numerically using centered second-order finite differences, staggered for U and ν_t, Runge-Kutta fourth-order time integration, and zero

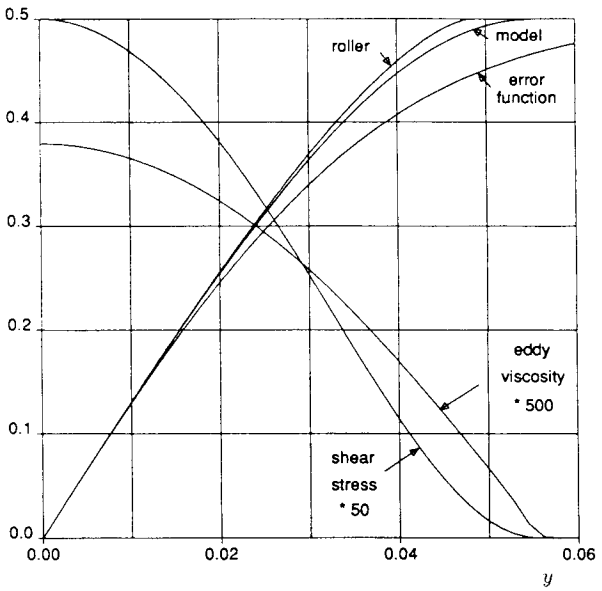

Fig. 2. – Profiles in a time-developing mixing layer. Normalized with velocity difference and time. Velocity profiles adjusted to the same slope at $y=0$.

values in the freestream. This artless treatment would rapidly reveal adverse numerical properties in the model. The growth of the layers was followed until a self-similar state was attained. The solutions exhibit the ramp structure at the edge of the turbulent region, as seen in the mixing-layer case in figure 2. The centered-difference solution cannot faithfully reproduce a weak solution at the front, but the error does not propagate.

Based primarily on the edge behavior, we favor a fairly diffusive member of our "plausible" range, namely $\sigma = 2/3$, $c_{b1} = 0.1355$, $c_{b2} = 0.622$. In the mixing layer it gives a velocity profile close to that associated with identical "rollers" of uniform vorticity (*Fig. 2*). Very low values of σ would be needed to bring it close to the error-function profile, which is a common approximation. That profile corresponds to uniform eddy viscosity, which cannot actually be achieved with low or zero freestream values. The hyperbolic-tangent profile, another common approximation, requires a diverging eddy viscosity outside the shear layer. In the wake the eddy viscosity is $0.046\,M$ on the centerline and $0.036\,M$ at the half-width, where M is the momentum of the wake. Experiments can be well matched with a uniform value of $0.044\,M$ [18]. Calculations of a plane jet yield a spreading rate about 38% higher than the experimental value. Thus, the jet/wake conflict is present, as with most models. In aerodynamics, the wake deserves a much higher priority.

II.3 – Near-wall region, high Reynolds number

In a boundary layer the blocking effect of a wall is felt at a distance through the pressure term, which acts as the main destruction term for the Reynolds shear stress. This suggests a destruction term in the transport equation for the eddy viscosity. Dimensional analysis leads to a combination $-c_{w1}\,(\nu_t/d)^2$ as a starting point, where d is the distance to the wall. The subscript w stands for "wall". This term is passive in free shear flows ($d \gg \delta$, so that the new term is much smaller than the diffusion term) and therefore does not interfere with our calibration up to this point. The Secundov model includes this type of term. The idea of a near-wall, but not viscous, "blocking" term is also in Hunt [19]. It is related to algebraic models, which take the smaller of two eddy viscosities. In these models the outer eddy viscosity scales with the boundary-layer thickness, and the inner eddy viscosity is given by the mixing length, $l \propto d$. In a classical log layer we have $S = u_\tau/(\kappa d)$ and $\nu_t = u_\tau\,\kappa d$. Equilibrium between the production and diffusion terms (all positive) and the destruction term is possible provided $c_{w1} = c_{b1}/\kappa^2 + (1 + c_{b2})/\sigma$.

Tests show that the model, when equipped with the destruction term, can produce an accurate log layer in a U^+ (y^+) plot (this requires an adequate treatment of the viscous region, which is described in § II,4.). On the other hand it produces too low a skin-friction coefficient in a flat-plate boundary layer. This shows that the destruction term as formulated above decays too slowly in the outer region of the boundary layer. To address this deficiency and allow a new calibration we multiply it by a non-dimensional function f_w, which equals 1 in the log layer. Note that c_{w1} is not negotiable (*i.e.*, we would not adjust the C_f at the expense of the log-law constants), and also that we were not able to obtain an accurate skin friction just by using the freedom left by the free-shear-flow calibration (*Fig. 1*). With the destruction term the model becomes

$$\frac{D\nu_t}{Dt} = c_{b1}\,S\nu_t + \frac{1}{\sigma}\left[\nabla.(\nu_t\,\nabla\nu_t) + c_{b2}\,(\nabla\nu_t)^2\right] - c_{w1}\,f_w\left[\frac{\nu_t}{d}\right]^2. \quad (4)$$

Secundov *et al.* did not follow the f_w route.

The choice of an argument for f_w was inspired by algebraic models, in which the mixing length plays a major role near the wall. This length can be defined by $l \equiv \sqrt{\nu_t/S}$ and we use the square of $l/\kappa d$ for convenience:

$$r \equiv \frac{\nu_t}{S\kappa^2\,d^2}. \quad (5)$$

Both r and f_w equal 1 in the log layer, and decrease in the outer region. Note that any dimensionally correct function of (ν_t, d, S) that reduces to $-c_{w1}\,\kappa^2\,u_\tau^2$ in a log layer would be as eligible as the destruction term we have inserted in (4). A satisfactory f_w function is

$$f_w(r) = g\left[\frac{1 + c_{w3}^6}{g^6 + c_{w3}^6}\right]^{1/6}, \qquad g = r + c_{w2}\,(r^6 - r). \quad (6)$$

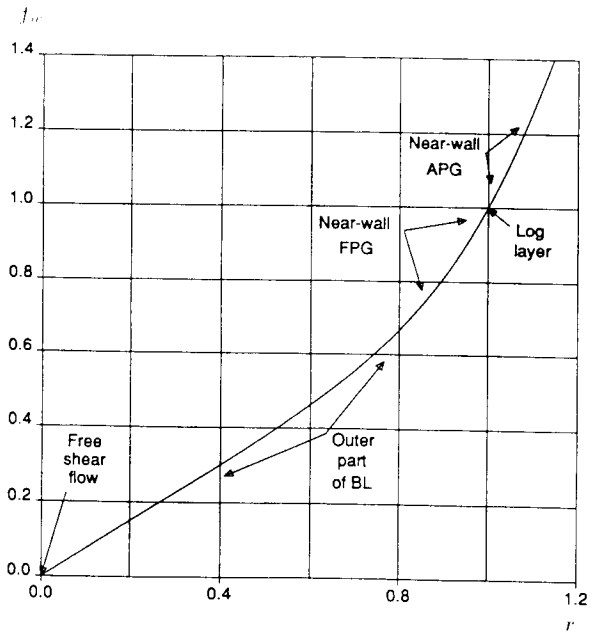

Fig. 3. – f_w function involved in the destruction term, Eq. (4-6). APG: adverse pressure gradient; FPG: favorable pressure gradient.

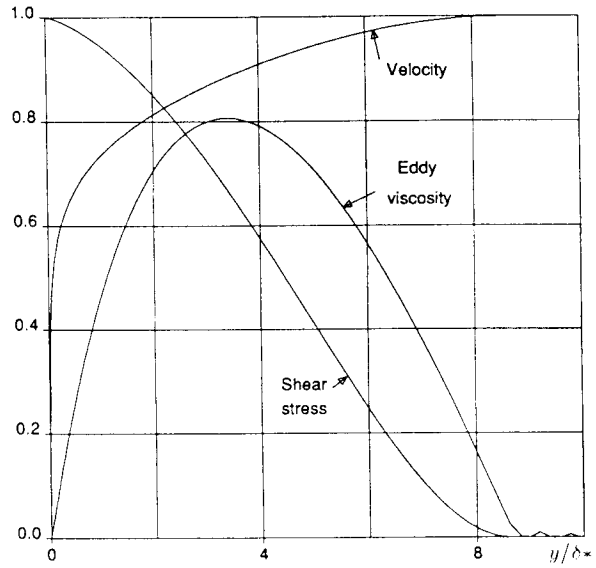

Fig. 4. – Profiles in a flat-plate boundary layer at $R_\theta \approx 10^4$, outer coordinates. U normalized with U_{edge}, τ with τ_{wall} and ν_t with $0.025 U_{edge}\delta^*$.

which is shown in figure 3. Results are most sensitive to the slope of f_w at $r=1$, which is controlled by c_{w2}. The step from g to f_w is merely a limiter that prevents large values of f_w, which could upset a numerical scheme and give an undeserved importance to the fact that S may vanish. The region $r > 1$ is exercised only in adverse pressure gradients, and then rarely beyond $r=1.1$. Having $f_w(0)=0$ is not essential, because in free shear flows the destruction term vanishes on account of the d^2 in its denominator. A reasonable value for c_{w3} is 2. We then calibrate c_{w2} to match the skin-friction coefficient in a flat-plate boundary layer (*Fig. 1*). We adopt the value of the CTTM, namely $C_f=0.00262$ at $R_\theta=10^4$ [16], which requires $c_{w2}=0.3$ for $\sigma=2/3$. The boundary-layer tests relied on a code written by Mr. D. Darmofal, of MIT, during a short stay at Boeing.

Figure 4 shows the velocity, eddy-viscosity, and shear-stress profiles in a flat plate boundary layer at $R_\theta \approx 10^4$. The traditional shape factor H is 1.31, the Clauser shape factor $G \equiv \sqrt{2/C_f}\,(H-1)/H$ is settled at 6.6, and the shape of the profile is satisfactory. Notice again the ramp structure of ν_t at the edge of the shear flow. The peak value of ν_t is $0.021 U_{edge}\ \delta^*$, compared with $0.0168 U_{edge}\ \delta^*$ in the Cebeci-Smith model [3]. Conversely, the Cebeci-Smith eddy viscosity is higher near $y/\delta^* = 1$.

Figure 5 shows the velocity profile in wall coordinates, illustrating the log layer and the smooth departure from that log law in the outer region. Again, the behavior in the viscous sublayer depends on the material in § II,4. The shape of the outer region appears good, showing that the destruction term and the f_w function are fair approximations, at least in this flow. The arrival at the freestream velocity is a little too abrupt, as it was in the mixing layer (*Fig. 2*).

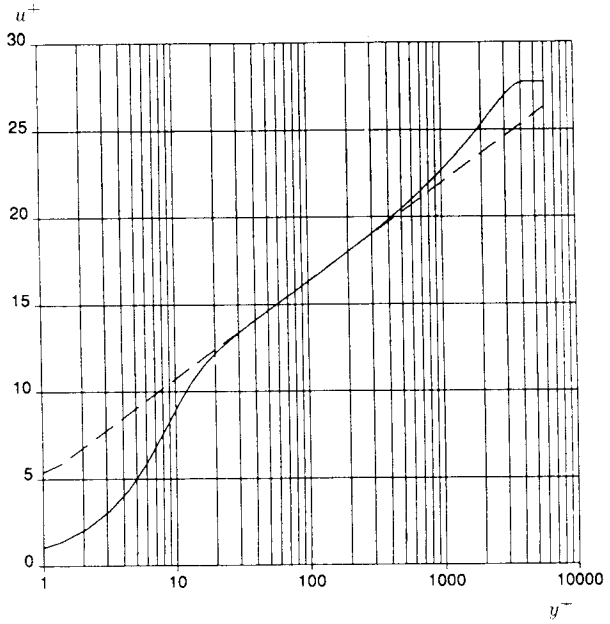

Fig. 5. – Velocity profile in a flat-plate boundary layer at $R_\theta \approx 10^4$, inner coordinates. — model; – – – log law.

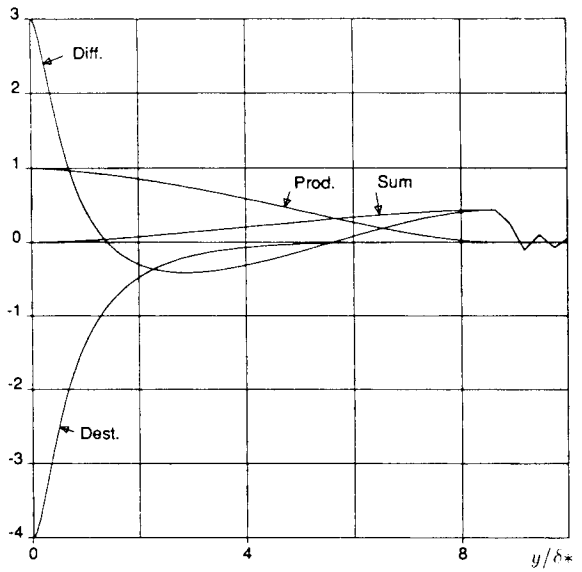

Fig. 6. – Eddy-viscosity budget in a flat-plate boundary layer. Normalized with $c_{b1}\tau_{wall}$.

The budget of ν_t is shown in *figure 6*. The sum (*i.e.*, $D\nu_t/Dt$) is positive throughout. It is zero at the wall, then roughly follows a ramp up to the edge of the turbulent region. Its outer part is representative of the outer part of either one of the free shear flows, including the vanishing contribution of the destruction term. The production is equal to the shear stress. In the outer part the diffusion is primarily responsible for the

advance of the turbulent front, in qualitative agreement with the budgets of "legitimate" turbulence quantities such as the kinetic energy. Near the wall the diffusion again makes a strong positive contribution, balanced by the destruction. This is not in qualitative agreement with the budget of the Reynolds shear stress (for which production and pressure destruction dominate). The ideal near-wall budget is, in the units of the figure: production = 1; diffusion ≈ 3; destruction ≈ -4. Note that it is not maintained far up into the layer at all; correspondingly, ν_t does not follow its ideal log-layer behavior ($\kappa y u_\tau$) far up either (*Fig. 4*). However this does not prevent a log layer from forming.

II.4 – Near-wall region, finite Reynolds number

In the buffer layer and viscous sublayer, additional notation is needed. Besides the wall units, y^+ and so on, we introduce $\tilde{\nu}$ which will equal ν_t except in the viscous region. We also use χ, which is in analogy with Mellor and Herring's notation [20], because from the wall to the log layer we have $\chi = \kappa y^+$.

We follow Baldwin and Barth [9] in choosing a transported quantity $\tilde{\nu}$ which behaves linearly near the wall. This is beneficial for numerical solutions: $\tilde{\nu}$ is actually easier to resolve than U itself, in contrast with ϵ, for instance. Therefore, the model will not require a finer grid than an algebraic model would. To arrive at this behavior we consider the classical law of the wall and devise near-wall "damping functions" that are compatible with known results. These functions are distinct from the f_w near-wall non-viscous destruction term.

The eddy viscosity ν_t equals $\kappa y u_\tau$ in the log layer, but not in the buffer layer and viscous sublayer. We define $\tilde{\nu}$ so that it equals $\kappa y u_\tau$ all the way to the wall. This leads to

$$\nu_t = \tilde{\nu} f_{v1}, \qquad f_{v1} = \frac{\chi^3}{\chi^3 + c_{v1}^3}. \tag{7}$$

The subscript v stands for "viscous". The f_{v1} function is borrowed from Mellor and Herring, except that we prefer the value $c_{v1} = 7.1$ to their 6.9, which we believe yields a low intercept for the log law. Note that there is no basis for (7) to apply at the edge of the turbulent region, where χ is also of order 1 and smaller. However, the eddy viscosity has little influence there, because of the absence of steep gradients.

The production term also needs attention. In it S is replaced with $\tilde{S}$, given by

$$\tilde{S} \equiv S + \frac{\tilde{\nu}}{\kappa^2 d^2} f_{v2}, \qquad f_{v2} = 1 - \frac{\chi}{1 + \chi f_{v1}}. \tag{8}$$

The function f_{v2} is constructed, just like f_{v1}, so that $\tilde{S}$ maintains its log-layer behavior ($\tilde{S} = u_\tau/(\kappa y)$) all the way to the wall. Equations (4-9) were derived by requiring the model to admit the law of the wall as a solution, and then eliminating u_τ from any of the formulas, in order for the model to be local. $\tilde{S}$ is singular at the wall, but $\tilde{\nu}$ is zero there, so that the production is well-behaved. Other quantities involved in the "inviscid" model are redefined in terms of $\tilde{\nu}$ instead of ν_t, for instance $r \equiv \tilde{\nu}/(\tilde{S}\,\kappa^2\,d^2)$.

We finally add a viscous diffusion term, consistent with a Dirichlet boundary condition at the wall, $\tilde{\nu} = 0$. This term too is based on an analogy, rather than a rigorous equation, and we pay little attention to a factor σ multiplying it. It vanishes in the ideal near-wall solution, since $\tilde{\nu}$ is linear. The transport equation has become

$$\frac{D\tilde{\nu}}{Dt} = c_{b1}\,\tilde{S}\tilde{\nu}$$

$$+\frac{1}{\sigma}\left[\nabla.((\nu+\tilde{\nu})\nabla\tilde{\nu}) + c_{b2}(\nabla\tilde{\nu})^2\right] - c_{w1} f_w \left[\frac{\tilde{\nu}}{d}\right]^2. \tag{9}$$

This equation now yields equilibrium ($D\tilde{\nu}/Dt = 0$) all the way to $d = 0$ in a classical law-of-the-wall situation. Furthermore, the evidence shows that this classical solution is a stable solution of the system made of the momentum equation and Eq. (9), as it has been obtained starting with a wide range of initial conditions. This includes the results of *figures 4 and 5*; in particular *figure 5* displays the viscous and buffer layers.

II.5 – Laminar region and trip term

II.5.1 – *Overview*

The final set of terms provides control over the laminar regions of the shear layers, which has two aspects: keeping the flow laminar where desired, and obtaining transition where desired. Codes with algebraic models usually have crude "off-on" devices or short ramps based on the grid index along the wall, and the Baldwin-Barth model has also been used that way (either by over-riding the model and setting the eddy viscosity to zero in the momentum equation, or by suppressing its production term). These devices do not help the convergence of the codes. In addition we require a device that is useable on unstructured grids, so a non-traditional approach is needed.

The boundary layer is "tripped". We use this word to mean that transition in the real flow is imposed by an actual trip, or that it is natural but its locations is known. *On no account should the model be trusted to predict the transition location. The responsibility of choosing transition points rests with the user of this turbulence model, whether through an educated guess or a separate prediction method.* This is true of all the models we know.

We refer to transition points in 2-D, and transition lines in 3-D. Often each 2-D body has two transition

points, but in some cases one of the boundary layers remains laminar all the way to the trailing edge, or to a sharp corner at which separation is unavoidable. The separated shear layer, however, must be turbulent, therefore a trip should be placed slightly upstream of the corner. Similarly, in 3-D the trip line may take widely different shapes. On an unswept wing it is likely to extend across the span at some fraction of the chord, but it could well be interrupted if part of the wing is laminar. On a turbulent swept wing, a short trip line wrapped around the leading edge near the root normally makes the whole wing turbulent. The propagation of the state of turbulence is qualitatively correct, in relation to its propagation in the real flow.

The specification of transition puts a new burden on the user; however, this burden has already been recognized by perceptive users of algebraic models, particularly when transitional separation bubbles are involved. The user has merely lost the option of ignoring transition and of running the case as "fully turbulent". He needs to ensure that the two trips (assuming the simple 2-D situation) bracket the stagnation point, which is not known exactly in advance. One recourse is to insert extra trips farther along the chord. We have verified that an already turbulent boundary layer is hardly disturbed when subjected to a further trip.

The following "turbulence index" is convenient to detect transition near a wall:

$$i_t \equiv \frac{1}{\kappa u_\tau} \frac{\partial \tilde{\nu}}{\partial n}. \tag{10}$$

These quantities are readily available, with u_τ defined as $u_\tau \equiv \sqrt{\nu|\omega|}$ in 3-D. In the Baldwin-Barth model the definition would be $c_\mu \nu (\partial \tilde{R}_T/\partial n)/(\kappa u_\tau)$. This index is close to 0 in a laminar region, and close to 1 in a turbulent region. It rises somewhat over 1 when the turbulent boundary layer approaches separation, at least in 2-D, revealing the upset of the near-wall region. The rapid diagnostic using i_t should be made routinely, and is particularly relevant if a calculation is thought to produce premature separation. It may be that the model failed to transition, or that laminar separation is unexpectedly occurring upstream of the trip. In either case the user must investigate the viscous physics of the solution, just like in an experiment.

II.5.2 – *Laminar region*

We described in § II,2. how $\tilde{\nu} = 0$ is an unstable solution (going in the direction of D/Dt) especially in thin shear layers. In a boundary-layer code the zero solution is easily maintained, but in a Navier-Stokes code exactly-zero values are rarely preserved, so that the model is "primed" by the streamwise diffusion term and by numerical errors upstream of the trip. It then transitions at a rate that depends on numerical details and has little to do with the boundary layer's true propensity to transition, as controlled by pressure gradient, suction, etc. We verified this behavior, and it is not acceptable.

A solution to this problem, which is purely numerical, is to alter the production term so that $\tilde{\nu} = 0$ is a stable solution, with a small basin of attraction. We take the convention that in the laminar region $\tilde{\nu}$ is less than about ν. If $\tilde{\nu} \leq \nu$, then $\nu_t \leq \nu/350$ because of the damping by f_{v1}, and the flow is effectively laminar. We multiply the production term by $(1\text{–}f_{t2})$, where

$$f_{t2} = c_{t3} \exp(-c_{t4} \chi^2). \tag{11}$$

The subscript t stands for "trip". In order for zero to attract $\tilde{\nu}$ down from values of about $\nu/2$, the following values are fair: $c_{t3} = 1.2$, $c_{t4} = 0.5$. In any case c_{t3} must be larger than 1. As for c_{t4}, it can be decreased several-fold, if a code still yields premature transition. The cross-over point of $(1\text{–}f_{t2})$, (*i.e.*, the bound of the basin of attraction), is at $\chi = \sqrt{\log(c_{t3})/c_{t4}}$. The value $c_{t4} = 0.5$ was small enough in our code, but no other users have exercised the trip term so far. Values of c_{t4} much smaller than 1 would start affecting the results in the turbulent region.

The values of c_{t3} and c_{t4} are the only ones that differ between the model as first published [22] and here. We discovered that the original values (*i.e.*, $c_{t3} = 1.1$, $c_{t4} = 2$) allowed premature transition in some of our cases. These cases had trips close to the leading edge, so the effect on the results was unnoticeable. The new values are safer, especially at high Reynolds numbers, and make essentially no difference once the flow is turbulent.

In order to still balance the budget near the wall we offset the change in the production term with an opposite change in the destruction term, involving f_{t2} [*see* Eq. (12) below]. Again we take an empirical approach, and have numerical evidence that it yields a stable system. A user that is doing boundary-layer calculations can leave the f_{t2} term out (*i.e.*, set $c_{t3} = 0$).

II.5.3 – *Trip term*

We wish to initiate transition near the specified trip points in a smooth manner, and to retain a local formulation. For this a source term is added that will be nonzero only in a small domain of influence. This domain should not extend outside the boundary layer. Not wanting to find this edge, nor violate invariance principles, we invoke the quantities ΔU and ω_t. ΔU is the norm of the difference between the velocity at the trip (*i.e.*, usually zero since the wall is not moving) and that at the field point we are considering. ω_t is the vorticity at the wall at the trip point. Upstream of the trip in a boundary-layer code, it is fair to take ω at the wall at the current station, since ω_t proper is not available yet. The thickness of the boundary layer is on the order of U_{edge}/ω_t. Recall that it is still laminar. We also introduce d_t, the distance from the field point to the closest trip point or line.

Dimensional analysis points to ΔU^2 as a starting point for the source term, and we arrive at

$$\frac{D\tilde{\nu}}{Dt} = c_{b1}\,[1 - f_{t2}]\,\tilde{S}\tilde{\nu} + \frac{1}{\sigma}\,[\nabla.((\nu + \tilde{\nu})\,\nabla\tilde{\nu}) + c_{b2}\,(\nabla\tilde{\nu})^2] - \left[c_{w1}\,f_w - \frac{c_{b1}}{\kappa^2}\,f_{t2}\right]\left[\frac{\tilde{\nu}}{d}\right]^2 + f_{t1}\,\Delta U^2, \quad (12)$$

with

$$f_{t1} = c_{t1}\,g_t\,\exp\left(-c_{t2}\,\frac{\omega_t^2}{\Delta U^2}\,[d^2 + g_t^2\,d_t^2]\right), \quad (13)$$

and $g_t \equiv \min(0.1, \Delta U/\omega_t \Delta x_t)$, where Δx_t is the grid spacing along the wall at the trip. The Gaussian in f_{t1} confines the domain of influence of the trip terms as needed; it is roughly a semi-ellipse. The magnitude is adjusted so that the integrated contribution for a particle crossing the domain of influence is on the order of $U_{\text{edge}}\delta$, as is ensured by typical algebraic models. The odd factor g_t is passive (*i.e.*, $g_t = 0.1$) in a situation with a very fine grid, but is quite active and necessary in practice. Without the grid dependence of g_t, the streamwise domain of influence of the trip would scale with the boundary-layer thickness, which can be very small in the laminar region. As a result, that domain would easily fall between two streamwise grid points, so that the trip would not be not felt at all. The g_t factor guarantees that the trip term is nonzero over a few streamwise stations. Like the f_{t2} term, the g_t factor is needed only for numerical reasons.

The value $c_{t2} = 2$ reflects typical values of $\delta\omega_t/U_{\text{edge}}$ in laminar boundary layers and is not a candidate for much adjustment. Tests indicate a wide range for c_{t1} between values so low that transition miscarries, and values so high that $\tilde{\nu}$ and the skin-friction overshoot. The value $c_{t1} = 1$ is well within that range; successful transition was obtained with 0.1 and with 10. It is possible that at very low Reynolds numbers c_{t1} would require more attention.

The growth of $\tilde{\nu}$ to nonlinear levels under the effect of the production term occurs in a few boundary-layer thicknesses (c_{b1} being roughly 0.13). This behavior mimics the secondary instabilities invoked by recent transition theories, which have growth rates on the order of $1/\delta$. However since the streamwise grid is often much coarser than δ, transition will still appear very steep to that grid. Thus, we have a formal advantage over the "off-on" models in that transition is a smooth process, but in practice this is marginal. Naturally, an adaptive grid will focus points at transition, and approach the ideal situation.

Figure 7 summaries § II,5. It shows the turbulence index i_t and the skin-friction coefficient (based on U_∞) near the leading edge on an airfoil for three calculations. The first two have $c_{t3} = 0$, which gives no precaution to avoid spurious transition, and no trip. They have different freestream values, $\chi_\infty = 10^{-2}$ and 10^{-4}, respectively. The index i_t is seen to rise gradually starting close to the stagnation point, at $x/c = 0.0016$, leading to transition at $x/c \approx 0.0060$ and $x \approx 0.0075$, respectively. Thus, transition is controlled by the highly arbitrary freestream value of $\tilde{\nu}$. In addition, "spontaneous" transition is occurring in a strong favorable pressure gradient, which is unphysical in a 2-D flow. The third calculation uses the complete model and a trip at $x/c = 0.03$. Initially, i_t decays as a result of the negative production term. Near $x/c = 0.027$ the trip terms becomes active, and the turbulence index jumps to 1, because it reflects only the near-wall region, which has a short length scale (on the order of ν/u_τ). The skin-friction coefficient rises more slowly, as a result of the larger length scale of the boundary layer as a whole (on the order of δ). Often the skin friction slightly overshoots that of the already-turbulent cases, which is qualitatively correct; farther downstream all the skin-friction curves converge.

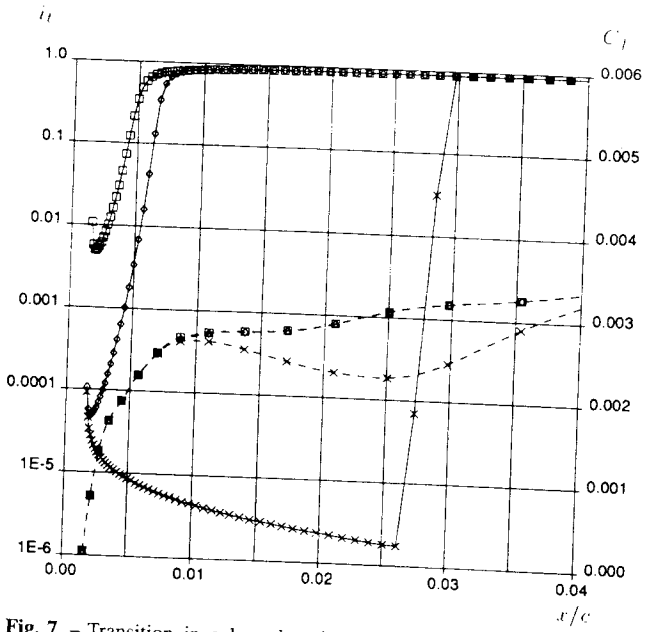

Fig. 7. – Transition in a boundary layer. □, fully turbulent, $\chi_\infty = 10^{-2}$; ◇, fully turbulent, $\chi_\infty = 10^{-4}$; ×, trip at $x/c = 0.03$. —, i_t; – – –, C_f.

Figure 7 shows that, with transport models, "fully turbulent" solutions actually conceal a laminar stretch of boundary layer of unpredictable length, although usually much shorter than would result from natural transition. In contrast, algebraic models are truly activated from the stagnation point on. The "fully turbulent" solutions may be satisfactory for simple cases, especially if the experiment used trips close to the leading edge (precisely to eliminate the influence of transition). The careful calculation of more complex cases, especially involving natural transition, requires

a full awareness of the state of the turbulence model, as provided by the i_t index.

II.6 – Initial and freestream conditions

Fair results have been obtained by initially setting $\tilde{\nu}$ uniformly to its freestream value. The turbulent viscosity emanates at the trips and spreads without noticeably degrading the convergence of the code. In the freestream the ideal value is zero. Some solvers may have trouble with this, for instance because of round-off errors. Freestream values $\tilde{\nu}_\infty \leq \nu/2$ are easily tolerable with the current c_{t3} and c_{t4} constants, and do not damage the laminar regions.

III – RESULTS

III.1 – Boundary-layer calculations

With zero pressure gradient, the model obeys the accepted Reynolds-number scaling, so the results shown at $R_\theta = 10^4$ ensure agreement with the theories. The model gives satisfactory results in attached boundary layers with pressure gradients, typical of the Stanford 1968 cases. We only present results for the sink flow and the Samuel-Joubert flow [21] as the other cases with moderate gradients show the same trend.

In the sink flow, with acceleration parameter $K \equiv \nu/U_{\text{edge}}^2 \, (dU_{\text{edge}}/dx) = 1.5 \times 10^{-6}$, we obtain $C_f = 0.00535$, $H = 1.35$, and $R_\theta = 760$. These results are well within the experimental range, which is about $C_f \in [0.0050, 0.0057]$, $H \in [1.35, 1.42]$, and $R_\theta \in [700, 800]$. The eddy-viscosity profile is atypical. Because of the lack of entrainment in the sink flow, it does not show a front at the edge of the boundary layer. Instead, it extends into the freestream region. This does not disturb the velocity profile, which is satisfactory both in terms of thickness and shape.

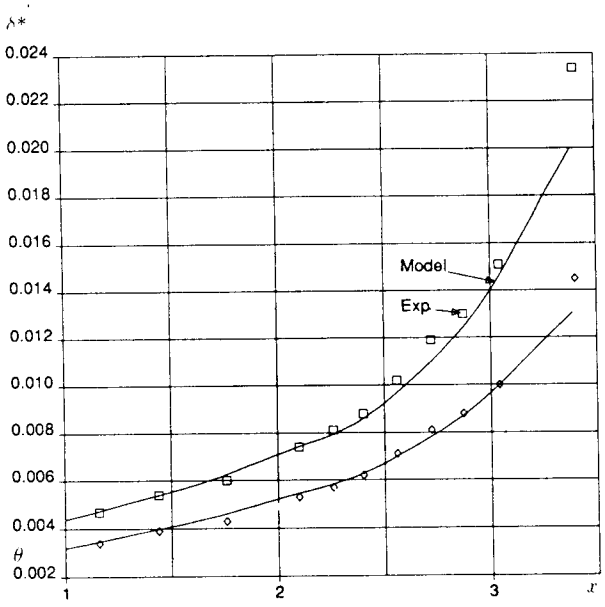

Fig. 9. – Momentum and displacement thickness in Samuel-Joubert flow, in meters.

In the Samuel-Joubert flow the agreement is rather good for the skin friction, *figure 8*, and the thickness, *figure 9*. The shape factors, however, are in mild disagreement even before the pressure gradient is applied. The experimental values for x between 1 and 2 m, $H \approx 1.39$, are surprisingly high, considering the weak pressure gradient and the Reynolds number, $R_\theta \approx 6{,}500$. Interestingly, the calculated shape factor

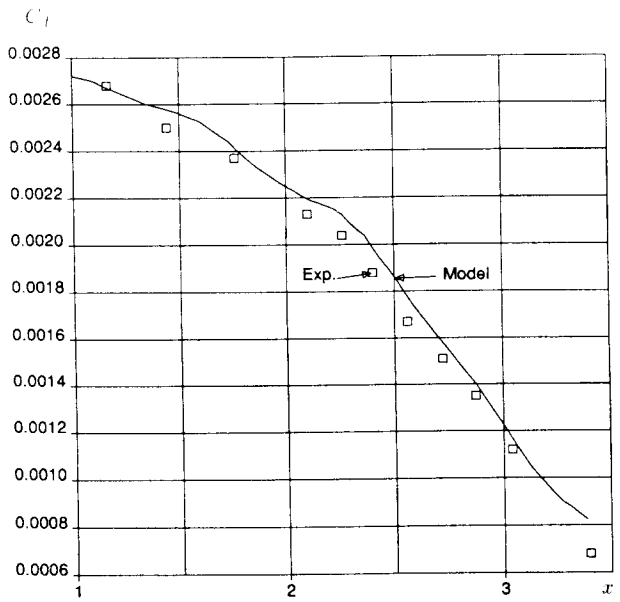

Fig. 8. – Skin-friction coefficient in Samuel-Joubert flow, based on $U_{\text{edge},0}$. x in meters.

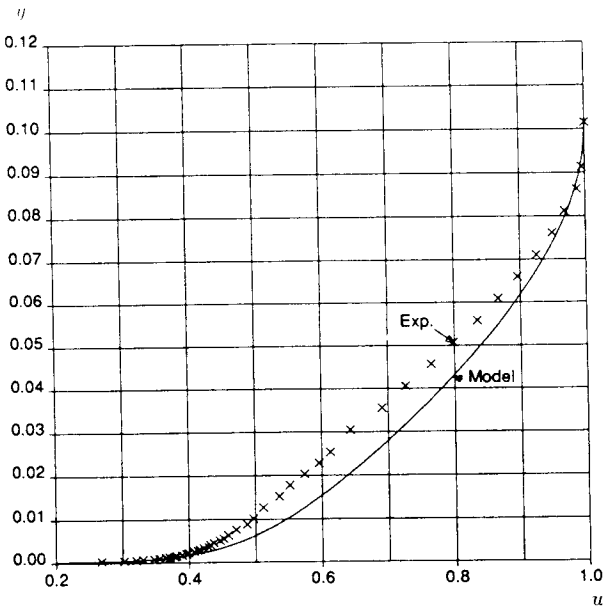

Fig. 10. – Velocity profile at $x = 3.4$ m in Samuel-Joubert flow. U normalized with U_{edge}. y in meters.

is catching up with the experimental one for $x > 3$ m. *Figure 10* shows the velocity at $x = 3.4$ m. The position of the boundary-layer edge is good, but the computed profile is fuller than the experimental profile. The shear-stress profiles in *figure 11* show good agreement for the outer values, but the near-wall agreement may be poor enough to partly explain the differences in the velocity profiles.

The Samuel-Joubert results suggest a mild tendency to underpredict the shape factor and thickness in adverse pressure gradients. This may make the model a little more resilient to separation than it would ideally be. The tendency is not as strong as with the Cebeci-Smith, Baldwin-Lomax, and k-ϵ models, but our comparison with experiment is not quite as good as that obtained by Menter with the Johnson-King and k-w models [10]. Both of these models have been finely tuned over years, with an emphasis on precisely this type of flow.

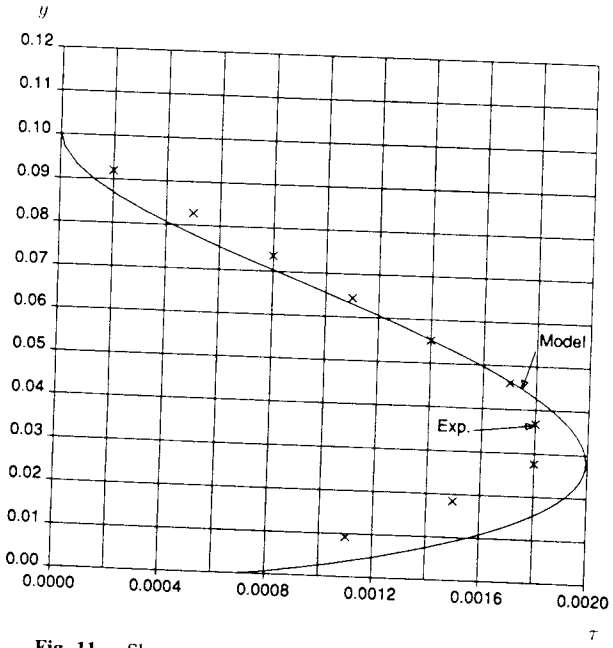

Fig. 11. – Shear-stress profile at $x = 3.39$ m in Samuel-Joubert flow. τ normalized with edge velocity. y in meters.

III.2 – Navier-Stokes calculations

We have developed a numerical procedure for solution of the turbulence transport model within a Navier-Stokes solver [22]. The solver for the turbulence model uses implicit time-marching, and discretizes advection terms by first-order upwinding and diffusion terms by second-order centered differencing. The implicit system is constructed and solved, using ADI with subiterations, to ensure a positive eddy viscosity at all points during the iteration procedure. The scheme is also unconditionally stable. We present three cases of the RAE 2822 airfoil; the first two have a sharp trailing edge with shock interactions of different strengths, and the third has a blunt trailing edge.

Navier-Stokes calculations for cases 6 and 10 on the RAE 2822 airfoil [23] were performed using the present model as well as the Baldwin-Lomax model, in Martinelli and Jameson's code [24], and the Johnson-King model in Swanson's code [25]. Results for each model were computed on 384×80 and 768×160 grids to exhibit numerical errors. These grids were generated by the elliptic method of Wigton [26].

All calculations for case 6 were performed at the same conditions: $M = 0.725$, $\mathrm{Re} = 6.5 \times 10^6$, a prescribed lift coefficient of $C_l = 0.743$, and transition trips at 3% chord. Results on the 768×160 grid are shown. All models converged solidly on both grids.

Figure 12 shows a comparison of surface pressures for case 6 obtained with the three turbulence models and experiment [23]. The shock for the present model is about 1.5% chord farther forward than in the experiment or as predicted with the other two models, but well within the scatter of various models as reported at the Viscous Transonic Airfoil Workshop (VTAW) [7]. The new model is farther from the experiment near the leading edge on the upper surface, but closer near the trailing edge on the lower surface. All the calculations reveal small pressure glitches near the trailing edge. With the new model on the fine grid, the angle of attack is 2.37°, the drag coefficient 0.0121, and the moment coefficient −0.091, compared with 2.92°, 0.0127, and −0.095 in the experiment, respectively.

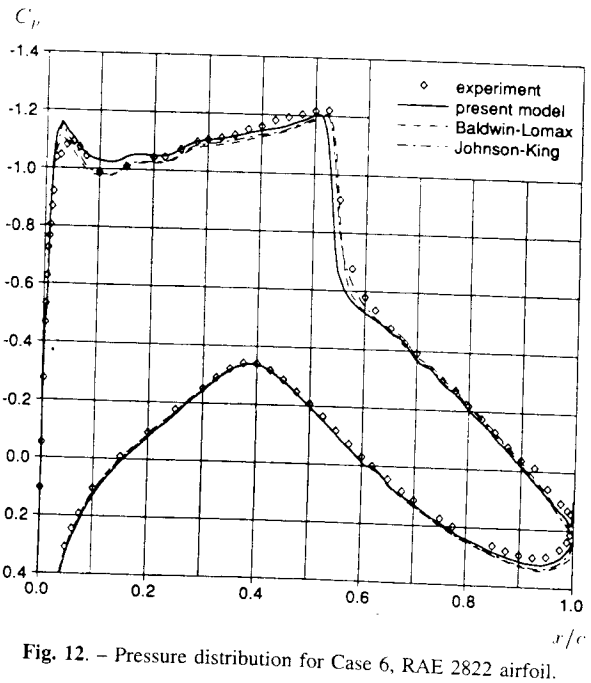

Fig. 12. – Pressure distribution for Case 6, RAE 2822 airfoil.

Figure 13 shows the upper-surface skin-friction coefficient for the same case. Between the three models there is a difference of up to 10% upstream of the shock, and similar but reversed differences downstream of it. The new model does not predict

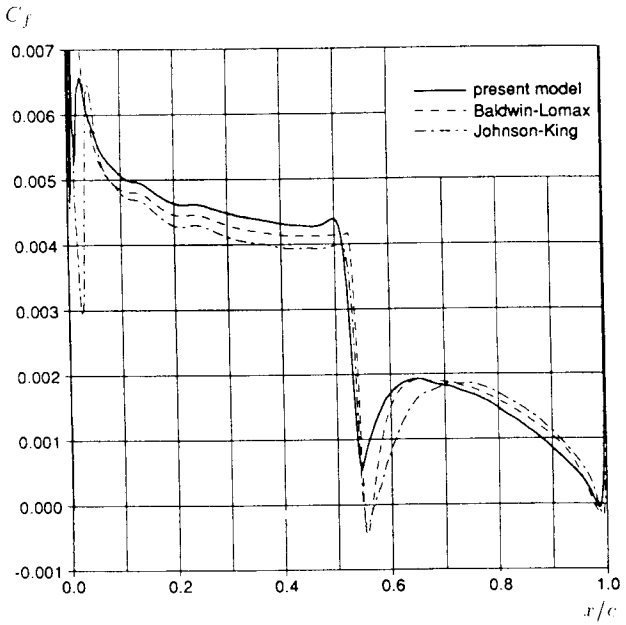

Fig. 13. – Skin-friction coefficient on upper surface for Case 6, RAE 2822 airfoil. C_f based on U_∞.

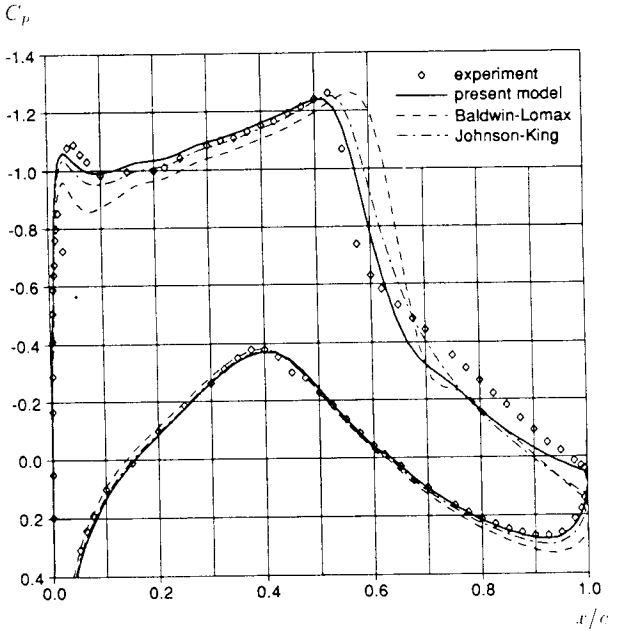

Fig. 14. – Pressure distribution for Case 10, RAE 2822 airfoil.

wall-shear reversal at the foot of the shock. The other two predict reversal, but only on the finest grid (768 × 160). Reversal was never predicted at the VTAW, where the finest grid used was 369 × 65. At the shock, the new model produces a larger step up for the boundary-layer thicknesses than with Baldwin-Lomax, resulting in a more forward position. Interestingly, the size of the displacement effect is not correlated with the occurence of reversal at the wall.

Flow conditions for the RAE 2822 Case 10 are $M=0.75$, $\mathrm{Re}=6.5\times10^6$, a prescribed lift coefficient of $C_l=0.743$, and trips at 3% chord. The new model obtained a steady solution on the 384 × 80 grid, but produced a limit cycle on the 768 × 160 grid. All the cyclic variation was in the separation bubble. The new model also produced a limit cycle on the 384 × 80 grid when the artificial dissipation in the Navier-Stokes solver was cut in half. The other two models produced steady solutions on both grids. Results are presented for all three models on the 384 × 80 grid.

As usual, Case 10 produces larger differences than Case 6. With our policy of matching the Mach number and lift coefficient, the new model gives a better answer than Baldwin-Lomax and slightly better than Johnson-King (*Fig. 14*). This is in terms of shock location and of pressures near the leading edge, for the upper surface, and near the trailing edge, for the lower surface. Our policy of matching the lift coefficient is not the only one possible, but it is very defendable, and was not chosen to enhance the new model's results. The differences in shock position would be essentially the same if the angle of attack were prescribed instead. All the models fail to agree with experiment for $x/c>0.6$, upper surface. The new model predicts a flattening pressure for $x/c>0.9$, upper surface, in qualitative disagreement with the experiment. The Johnson-King model has shown the same trend, but not as strongly and only in Coakley's implementation [7]. The Baldwin-Barth model also produces the flattening [9].

This behavior of the C_p may be correlated with that of the skin-friction coefficient, figure 15. Downstream of the shock, the experiment and our Johnson-King

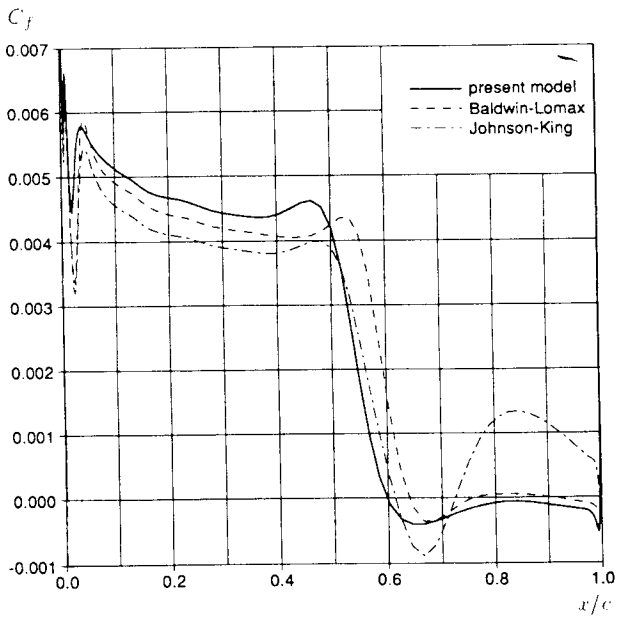

Fig. 15. – Skin friction coefficient on upper surface for Case 10, RAE 2822 airfoil. C_f based on U_∞.

results show the skin friction returning to strong positive values. The flow reattaches firmly. The Baldwin-Lomax results show weakly positive skin friction over a short stretch. With the new model the skin friction grazes zero before again taking small negative values. The limit cycle behavior on the fine grid shows an oscillation between slightly negative and slightly positive skin friction near $x/c=0.8$. For Case 10, with the new model on the 384×80 grid, the angle of attack was 2.52°, the drag coefficient 0.0238, and the moment coefficient −0.104, compared with 3.19°, 0.0242, and −0.106 in the experiment, respectively.

The blunt-trailing-edge airfoil is RAE 2822, truncated at 94% of the original chord (base height 1.14% chord). Similar calculations were performed by Stanaway, McCroskey and Kroo [6]. Our objective is to explore the behavior of the model and of the numerics at corner-induced separation, with high-lift applications in mind. Accordingly we choose Case 1 [27] which is subcritical: $M=0.676$, $\mathrm{Re}=5.4 \times 10^6$, and lift coefficient $C_l=0.451$. Calculations are performed on medium and fine two-block grids. The fine grid consists of a 768×160 C-grid block around the airfoil and a 128×64 block downstream of the blunt trailing edge. Strong convergence of the iterations is obtained, and solution glitches are less severe than with the sharp trailing edge. The angle of attack is 2.035°, the drag coefficient 0.0097, and the moment coefficient −0.061, compared with 2.45°, 0.0098, and −0.060 in the experiment, respectively.

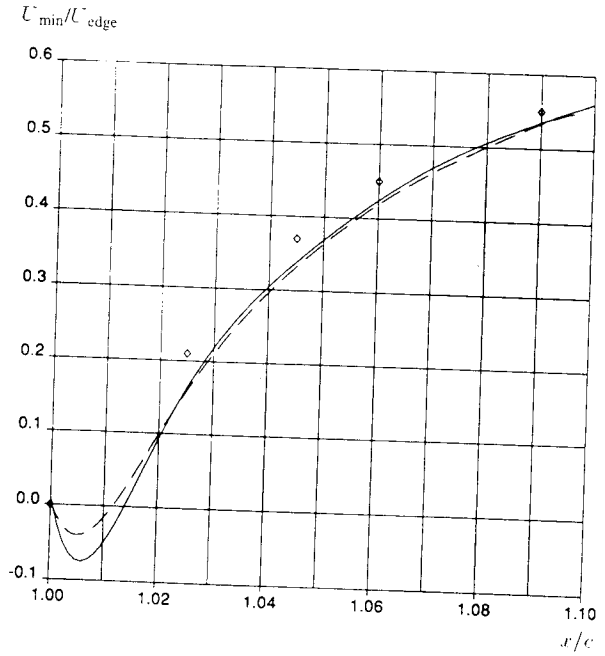

Figure 16. – Minimum velocity in wake for Case 1, blunt RAE 2822 airfoil. ◊ experiment, — 768×160 grid, – – – 384×80 grid.

Figure 16 shows the minimum velocity in the wake which is in fair agreement with the experiment [27]. In another example of slow grid convergence of the detail features in the flow, the amplitude of the backflow doubles between the 384×80 grid and the 768×160 grid. The region with negative velocities extends a little over one base height (*i.e.*, 1.35% on the fine grid) beyond the trailing edge. The report on the experiment also shows about 1.2 step heights, but the interpolation is debatable in that the $U=0$ line is shown with an apex, probably due to the understandable sparsity of the measurements. The computed curve is shifted by about 0.5% chord downstream; the slopes agree very well. This suggests that the model not only gives an accurate growth rate for a fully-developed wake (per its calibration), but is also fairly accurate for a "young", asymmetric one. The near wake of a wing, which is combined with a mixing layer, is still a different problem; nevertheless, we expect the model should also be able to treat it well.

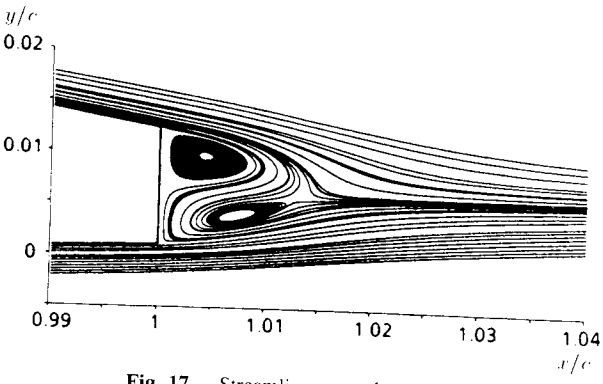

Fig. 17. – Streamlines near the trailing edge for Case 1, blunt RAE 2822 airfoil.

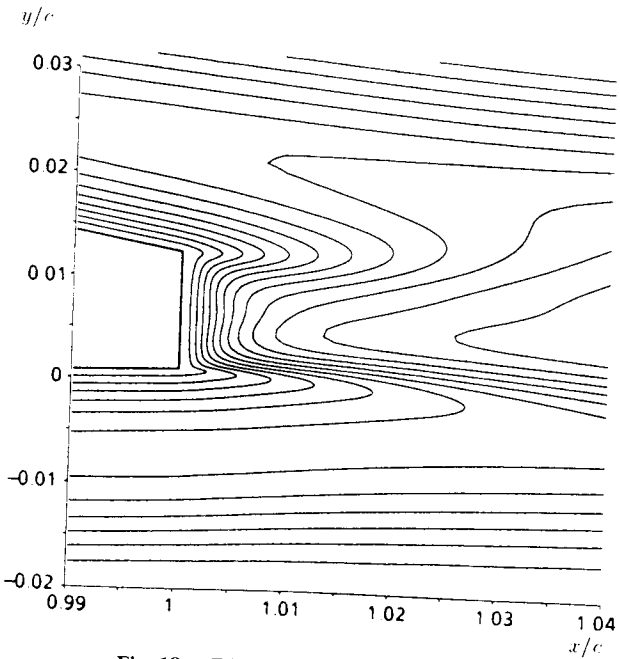

Fig. 18. – Eddy-viscosity contours near the trailing edge for Case 1, blunt RAE 2822 airfoil.

Figure 17 shows streamlines (but not equally-spaced stream-function contours). Their pattern is unexpected, being rather asymmetric and indicating "reattachment" of an upper-surface streamline near the mid-point of the base. There are three half-saddles, one saddle, and two foci. This was also obtained by Stanaway *et al.* and sharply differs from the "educated guess" made, for instance, in [28]. That guess assumes that the streamlines connected to the three half-saddles meet at the full saddle, isolating the two foci. There is no reason for such a pattern to occur in the absence of symmetry, and it is not stable. The saddle and the lower focus could also eliminate each other under other conditions. In fact a referee pointed out that such an elimination had occurred as the grid was refined in his Navier-Stokes calculation. We certainly cannot rule out such a grid effect in view of our *figure 16*. A single-focus pattern was also indicated by the referee's experiments, adding much weight to his remark. Note that the more surprising feature, namely the reattachment of the upper-surface streamline on the base, is present in any case. Note also that streamline patterns can overstate the importance of regions with low velocity and little dynamical significance.

Figure 18 shows eddy-viscosity contours. Continuity between the grid blocks, which is hard to achieve with algebraic models, is of course observed. The eddy viscosity blends its boundary-layer behavior (as in *Fig. 4*) into its wake behavior (a bell-shaped distribution).

III.3 – Summary of the results

We have exercised the model outside its domain of calibration and with the Navier-Stokes equations, instead of just the boundary-layer equations. Its compatibility with unstructured grids has now been exploited by Anderson and Bonhaus [29]. Its implementation in three dimensions is fully defined, as confirmed by Rumsey and Vatsa [30]. In a few cases with shock-induced separation the new model yielded a limit cycle, with a pulsation of the bubble, when the algebraic models yielded steady solutions. Since time-accurate solutions are expensive, steady solutions may be greeted as successes whether they are physically correct or not [22]. The model seems to be quite "friendly" to the relaxation process, without any attention being paid to the initial condition [6]. Difficulties have been reported along the wake cut in a C-grid code that usually runs with zero eddy viscosity, given by a crude algebraic model, on the grid cut (K. Kusunose, personal communication). The present model does not have this unphysical behavior, and in that code the combination of very fine grid and finite eddy viscosity prevents convergence. The situation improves if the normal grid spacing along the grid cut is loosened. Overall, the model appears robust enough to be implemented by independent users, in a variety of codes and physical situations, and it should be particularly attractive to unstructured-grid users.

The accuracy so far is consistent with our expectations. The model's response to gradual or steep pressure gradients, and to the removal of the blocking effect of the wall, is very encouraging. The post-shock reattachment in an adverse pressure gradient has proven to be difficult for the model. Menter also reported somewhat disappointing results over a backward-facing step, traced to an excessively-rapid build-up of the shear stress (personal communication). This weakness also afflicts the k-ϵ model, and may respond to a modification of the d and f_w functions and to a streamline-curvature term. The quality of our results with the blunt trailing edge indicate that this problem cannot be very severe. It appears that the calibration cases are indeed representative enough of the flows of interest to ensure decent performance in non-trivial situations, and to warrant an extensive validation of the model in its present form.

REFERENCES

[1] Baldwin B. S. and Lomax H. – Thin layer approximation and algebraic model for separated turbulent flows, AIAA-78-257.

[2] Michel R., Quemard C. and Durant R. – Application d'un schéma de longueur de mélange à l'étude des couches limites d'équilibre, ONERA Note Technique n° 157, 1969.

[3] Cebeci T. and Smith A. M. O. – A finite-difference method for calculating compressible laminar and turbulent boundary layers, *J. Basic Eng.*, **92**, No. 3, 523-535.

[4] Johnson D. A. and King L. S. – A mathematically simple turbulence closure model for attached and separated turbulent boundary layers, *AIAA J.*, 1985, **23**, No. 11, 1684-1692.

[5] Mavriplis D. J. – Algebraic turbulence modeling for unstructured and adaptive meshes, AIAA-90-1653.

[6] Stanaway S. K., McCroskey W. J. and Kroo I. M. – Navier-Stokes analysis of blunt trailing edge airfoils, AIAA-92-0024.

[7] Holst T. L., Viscous transonic airfoil workshop. Compendium of results, AIAA-87-1460.

[8] Baldwin B. S. and Barth T. J. – A one-equation turbulence transport model for high Reynolds number wall-bounded flows, NASA TM 102847, 1990.

[9] Baldwin B. S. and Barth T. J. – A one-equation turbulence transport model for high Reynolds number wall-bounded flows, AIAA-91-0610.

[10] Menter F. R. – Performance of popular turbulence models for attached and separated adverse pressure gradient flows, *AIAA J.*, 1992, **30**, No. 8, 2066-2072.

[11] Bradshaw P., Ferriss D. H. and Atwell N. P. – Calculation of boundary-layer development using the turbulent energy equation, *J. Fluid. Mech.*, 1967, **28**, 3, 593-616.

[12] Nee V. W. and Kovasznay L. S. G. – Simple phenomenological theory of turbulent shear flows, *Phys. Fluids*, 1969, **12**, No. 3, 473-484.

[13] Secundov, Smirnova, Kozlov and Gulyaev. – One-equation eddy viscosity model (modified L.S.J.

Kovasznay model). Short summary of the equations. Personal communication, 1990.
[14] Mitcheltree R. A., Salas M. D. and Hassan H. A. – One-equation turbulence model for transonic airfoil flows, *AIAA J.*, 1990, **28**, No. 9, 1625-1632.
[15] Johnston L. J. – Solution of the Reynolds-averaged Navier-Stokes equations for transonic aerofoil flows, *Aeronautical J.*, 1991, 253-273.
[16] Bradshaw P., Launder B. E. and Lumley J. L. – Collaborative testing of turbulence models, AIAA-91-0215.
[17] Towsend A. A. – The structure of turbulent shear flow. Cambridge University Press, New York, 1976.
[18] Schlichting H. – Boundary-layer theory, McGraw-Hill, New York, 1979.
[19] Hunt J. C. R. – Turbulence structure in thermal convection and shear-free boundary layers, *J. Fluid Mech.*, 1984, **138**, 161-184.
[20] Mellor G. L. and Herring H. J. – Two methods of calculating turbulent boundary layer behavior based on numerical solution of the equations of motion. Proc. Conf. Turb. Boundary Layer Pred., Stanford, 1968.
[21] Samuel A. E. and Joubert P. N. – A boundary layer developing in an increasingly adverse pressure gradient., *J. Fluid Mech.*, 1974, **66**, 3, 481-505.
[22] Spalart P. R. and Allmaras S. R. – A one-equation turbulence model for aerodynamic flows, AIAA-92-0439.
[23] Cook P. H., McDonald M. A. and Firmin M. C. P. – Aerofoil RAE 2822 – Pressure distributions, and boundary layer and wake measurements, AGARD-AR-138, 1979.
[24] Martinelli L. and Jameson A. – Validation of a multigrid method for the Reynolds averaged equations, AIAA-88-0414.
[25] Swanson R. C. and Turkel E. – Artificial dissipation and central difference schemes for the Euler and Navier-Stokes equations, AIAA-87-1107, 1987.
[26] Wigton L. B. – High quality grid generation using Laplacian sweeps. Fourth International Symposium on Computational Fluid Dynamics, U.C. Davis, 1991, 1222-1228.
[27] Cook P. H. and McDonald M. A. – Wind tunnel measurements in the boundary layer and wake of an airfoil with a blunt base at high subsonic speeds, RAE Tech. Rept. 84002, 1984.
[28] Henne P. A. and Gregg R. D. – A new airfoil design concept, AIAA-89-2201-CP.
[29] Anderson W. K. and Bonhaus D. L. – Navier-Stokes computations and experimental comparisons for multielement airfoil configurations, AIAA-93-0645.
[30] Rumsey C. L. and Vatsa V. N. – A comparison of the predictive capabilities of several turbulence models using upwind and central-difference computer codes, AIAA-93-0645.

Acknowledgements

The initial work was performed by the first author while an employee of NASA Ames Research Center. Dr. L. Wigton reviewed the manuscript and ran some of the cases. Mr. W.F. Nouss reviewed the manuscript. Ms. W. Wilkinson provided some of the files. We have benefited from comments by Drs. Baldwin, Barth, Birch, Bradshaw, Jou, McLean, Menter, Speziale, and Vandromme. These comments do not constitute endorsements.

APPENDIX: SUMMARY OF THE MODEL. VERSION Ia

We solve the Reynolds-averaged Navier-Stokes equations and a transport equation for the turbulence model. The Reynolds stresses are given by $-\overline{u_i\,u_j} = 2\nu_t\,S_{ij}$. The eddy viscosity ν_t is given by

$$\nu_t = \tilde{\nu}\,f_{v1}, \qquad f_{v1} = \frac{\chi^3}{\chi^3 + c_{v1}^3}, \qquad \chi \equiv \frac{\tilde{\nu}}{\nu}. \quad \text{(A1)}$$

ν is the molecular viscosity. $\tilde{\nu}$ obeys the transport equation

$$\begin{aligned}\frac{D\tilde{\nu}}{Dt} =& c_{b1}\,[1 - f_{t2}]\,\tilde{S}\tilde{\nu} \\ &+ \frac{1}{\sigma}\,[\nabla.((\nu + \tilde{\nu})\,\nabla\tilde{\nu}) + c_{b2}\,(\nabla\tilde{\nu})^2] \\ &- \left[c_{w1}\,f_w - \frac{c_{b1}}{\kappa^2}\,f_{t2}\right]\left[\frac{\tilde{\nu}}{d}\right]^2 + f_{t1}\,\Delta U^2. \quad \text{(A2)}\end{aligned}$$

Here

$$\tilde{S} \equiv S + \frac{\tilde{\nu}}{\kappa^2\,d^2}\,f_{v2}, \qquad f_{v2} = 1 - \frac{\chi}{1 + \chi f_{v1}}, \quad \text{(A3)}$$

where S is the magnitude of the vorticity, and d is the distance to the closest wall.

The function f_w is

$$\left.\begin{aligned} f_w &= g\left[\frac{1 + c_{w3}^6}{g^6 + c_{w3}^6}\right]^{1/6}, \\ g &= r + c_{w2}\,(r^6 - r), \qquad r \equiv \frac{\tilde{\nu}}{\tilde{S}\,\kappa^2\,d^2}. \end{aligned}\right\} \quad \text{(A4)}$$

For large r, f_w reaches a constant, so large values of r can be truncated to 10 or so.

The wall boundary condition is $\tilde{\nu} = 0$. In the freestream 0 is best, provided numerical errors do

not push $\tilde{\nu}$ to negative values near the edge of the boundary layer (the exact solution cannot go negative). Values below $\nu/10$ will be acceptable. The same applies to the initial condition.

In some codes a portion of the solid surface, typically the fuselage, is treated with a free-slip condition while another portion, typically the wing, is treated with a no-slip condition. For $\tilde{\nu}$, the appropriate condition on the free-slip surface is a Neumann condition (zero normal derivative). In addition, the free-slip wall points are not included in the search when d is computed for the field points.

The f_{t2} function is

$$f_{t2} = c_{t3} \exp(-c_{t4} \chi^2). \quad \text{(A5)}$$

The trip function f_{t1} is as follows: d_t is the distance from the field point to the trip, which is on a wall, ω_t is the wall vorticity at the trip, and ΔU is the difference between the velocity at the field point and that at the trip. Then $g_t \equiv \min(0.1, \Delta U/\omega_t \Delta x_t)$ where Δx_t is the grid spacing along the wall at the trip, and

$$f_{t1} = c_{t1} g_t \exp\left(-c_{t2} \frac{\omega_t^2}{\Delta U^2} [d^2 + g_t^2 d_t^2]\right). \quad \text{(A6)}$$

The constants are $c_{b1} = 0.135,5$, $\sigma = 2/3$, $c_{b2} = 0.622$, $\kappa = 0.41$, $c_{w1} = c_{b1}/\kappa + (1 + c_{b2})/\sigma$, $c_{w2} = 0.3$, $c_{w3} = 2$, $c_{v1} = 7.1$, $c_{t1} = 1$, $c_{t2} = 2$, $c_{t3} = 1.2$, $c_{t4} = 0.5$ (note again that c_{t3} and c_{t4} are different from those in Version I [22]). Turbulent heat transfer obeys a turbulent Prandtl number (not to be confused with σ) equal to 0.9. In a compressible flow, equations (A1-A6) have been applied directly. Density variations have only a weak influence on turbulence in the slightly supersonic boundary layers we have treated so far.